The experiment and validation of sea ice concentration AMSR – E retrieval algorithm in polar region

SU Jie[1], HAO Guanghua[1], YE Xinxin[1,2], WANG Weibo[1]

1. *Key Laboratory of Physical Oceanography of State Education Ministry, Ocean University of China, Qingdao* 266100, *China*;
2. *Department of Atmospheric and Oceanic Science, School of Physics, Peking University, Beijing* 100871, *China*

Abstract: Sea ice concentration is an important parameter for polar sea ice monitoring. Currently, the highest resolution microwave-detected sea ice concentration gridded product is provided by University of Bremen, which is derived by the Arctic Radiation and Turbulence Interaction Study (ARTSIST) Sea Ice (ASI) algorithm based on 89 GHz Advanced Microwave Scanning Radiometer for Earth Observing System (AMSR-E) data. For the purpose of providing the first generation Chinese sea ice remote sensing product for polar regions, we implemented a series of experiments including the interpolation algorithm, tie-points, and the weather filter based on the ASI algorithm for AMSR-E 89 GHz data. The main parameters, tie-points threshold value of pure ice (P_1) and pure water (P_0) of ASI algorithm in the Arctic region were statistically analyzed throughout year 2009. The results showed that the yearly average value of P_1 was 10.0 K, and that of P_0 was 46.67 K in the pure ice and pure water typical regions of Arctic. The retrieved values of ice concentration is sensitive to P_1 and P_0 when the differences of tie-points value are larger than 2 K. The effects of P_1 and P_0 on the ice concentration also changed for different P values. The calculation fomula was amended based on the statistic tie points. The sea ice concentration inversion fields in Arctic region of whole 2009 was obtained and compared with the products of University of Bremen. Furthermore, 12 cloud-free samples were selected from the visible band of Moderate-resolution Imaging Spectroradiometer (MODIS) image in Bering Sea and Chukchi Sea, and the derived sea ice concentration of MODIS data is averaged in the AMSR-E grid to validate the AMSR-E sea ice concentration. The comparisons of these samples showed that the error of our results is slightly less than that of University of Bremen's product with the spatial average error and spatial average absolute error of 3.84% and 10.83%, respectively.

Key words: AMSR-E, ice concentrations, retrieval algorithm, validation, polar region

CLC number: TP701/P731.15 **Document code:** A

Citation format: **Su J, Hao G H, Ye X X and Wang W B. 2013. The experiment and validation of sea ice concentration AMSR-E retrieval algorithm in polar region. Journal of Remote Sensing, 17(3): 495 – 513**

1 INTRODUCTION

The polar region is an indicator of global climate. As global warming intensified, sea ice, as an important climatic factor, gains an increasing amount of attention in monitoring and research programs. Sea ice concentration indicates the space-intensive extent of sea ice, which equals to the area percentage occupied by sea ice in a range. It is not only one of the important parameters which describe the sea ice characteristics, but also the input variable of the atmosphere and ocean circulation models. Currently, active and passive microwave radiometers, visible and infrared radiometers and imaging spectrometers are the main satellite sensors used in deriving large area sea ice concentration. The microwave data has become an important resource for polar sea ice monitoring due to its good temporal and spatial continuity, and its freedom from limitations associated with polar night, rain and fog.

The resolution of satellite data and the retrieval algorithm are among the primary factors that determine the accuracy of the sea ice concentration retrieval. Using the 89 GHz frequency data of AMSR-E boarded on the Aqua satellite (launched in May 2002), University of Bremen has derived 6.25 km resolution sea ice concentration product, which has the highest resolution among the published microwave sea ice concentrations grid products (Spreen, et al., 2008). Present sea ice concentration algorithms for the AMSR-E microwave data are mostly based on the algorithms for the lower-resolution Special Sensor Microwave Imager (SSM/I) data. Andersen, et al. (2007) summarized seven sea ice concentration retrieval algorithms designed for the SSM/I data. Among the present most commonly used algorithms, NASA-Team algorithm (Cavalieri, et al., 1984) and Bootstrap algorithm (Comiso, 1986, 1995) are based on the 19 GHz and 37 GHz low-resolution data; NASA-Team2 Algorithm (Markus & Cavalieri, 2000), SEA LION algorithm (Kern, et al., 2001a, 2001b) and ARTSIST Sea Ice (ASI) algorithm (Kaleschke, et al., 2001) include the SSM/I 85 GHz band da-

Received: 2012-02-14; **Accepted:** 2012-09-24; **Version of record first published:** 2012-10-01

Foundation: National High Technology Research and Development Program of China (863 Program) (No. 2008AA121701)

First author biography: SU Jie (1966—), female, Ph. D., associate professor, her research interests are ice-ocean coupled model and sea ice remote sensing. She has published over 40 papers. E-mail: sujie@ouc.edu.cn

ta, and they can provide 12.5 km resolution sea ice concentration grid data. ASI algorithm was developed at near 90 GHz bands data during the Arctic Radiation and Turbulence Interaction Study (ARTSIST) research projects (Svendsen, et al., 1987). Compared with other algorithms using near 85 GHz bands data, the ASI algorithm does not need additional input data but has a similar accuracy (Kern, et al., 2003).

AMSR-E offers approximately 6 km × 4 km spatial resolution at 89 GHz, nearly three times of the resolution of the standard sensor SSM/I at 85 GHz (15 km × 13 km). Therefore, a fter AMSR-E data became available, the ice concentration algorithms base on SSM/I 85 GHz data were quickly applied to the AMSR-E 89 GHz band data. The sea ice concentration retrieved from the AMSR-E data based on algorithms of ASI (Spreen, e t al. 2008), NASA-Team2, AMSR Bootstrap Algorithm (ABA, Comiso, et al., 2003) are compared with the ship observations obtained in the ARK-XIX/1 study (March—April, 2003), and the ARK-XX/2 (July—August, 2004), and the correlation coef-ficients were 0.80, 0.79 and 0.81 respectively; during 2002 to 2006 the deviation of the ASI results (6.25 km) from the NASA-Team2 results (12.5 km) was $-2 \pm 8.8\%$, while that of the ABA results (12.5 km) was $1.7 \pm 10.8\%$, reflecting the ASI algorithm's validity (Spreen, et al., 2008). Using 89 GHz data, ASI algorithm can provide 6.25 km sea ice concentration, which twice higher than the NASA-Team 2 and ABA algorithms' resolution.

Interpolation of the original track data to the product grid is the basic steps of the inversion process. The interpolation algorithm will make certain difference on the results of daily sea ice concentration inversion field. Although the ASI algorithm has been proposed (Spreen, et al., 2008), the detailed data pre-p rocessing steps, especially the interpolation algorithm of source data are not available. Besides, the pure ice and pure water tie-points (the thresholds of polarization difference between vertical and horizontal polarization brightness temperatures) used in the ASI algorithm were determined by minimizing the deviation of the sea ice concentration derived with the ASI algorithm and that derived with the ABA algorithm (Comiso, et al., 2003). This a pproach will undoubtedly make the inversion results of the ASI algorithm being affected by the accuracy of ABA algorithm i nversion results. Additionally, compared with the low frequency data, the 89 GHz band data is obviously influenced by the a tmospheric cloud liquid water, rain droplets and water vapor and snow particle density on the ice surface, so weather filter processing is needed in the ASI algorithm (Spreen, et al., 2008). It is therefore necessary to validate and improve the ASI algorithm. Relying on the National High Technology Research and Development Program of China, "Polar sea ice and ocean process remote sensing technology", the remote sensing retrieval algorithms of 16 polar sea ice and ocean parameters, including sea ice concentration are appling or developing by Chinese r esearchers, in order to achieve the Chinese first generation remote sensing quasi-operationally products in polar regions. This paper aims at testing the ASI algorithm using AMSR-E 8 9 GHz band microwave data, include the interpolation algorithm, tie-points and the effects of weather filters; the tie-points' impact on retrieval results are also discussed and the values of tie-points were statistically amended. Furthermore, the sea ice concentrations derived from the MODIS visible data was also used to validate the microwave data results using ASI algorithm.

2 DATA SET

AMSR-E Level-2A global swath spatially-resampled brightness temperature data from the National Snow and Ice Data C enter (NSIDC) [1] was taken as the main data source. AMSR-E on the Aqua platform launched in May, 2002 measures radiances of six channels at central frequencies 6.9 GHz, 10.7 GHz, 1 8.7 GHz, 23.8 GHz, 36.5 GHz, and 89.0 GHz with both horizontal and vertical polarizations. The analogous AMSR-E ice concentration data sets, i. e., AMSR-E ice concentration products provided by University of Bremen (Spreen, et al., 2008) were downloaded for comparison.

The visible light remote sensing data from the MODIS sensor was used to validate AMSR-E results. The MODIS sensor can provide images of totally 36 separated spectral bands ranging in wavelength from 0.4—14.5 μm. The viewing swath width is 2330 km. The realtime surface conditions of land and sea are clearly shown and documented. In this work, the band-2 data in MODIS L1B data with 250 m resolution was chosen in validation process. Ice concentration was retrieved using the tie-point algorithm (Steffen, et al., 1991). The processing procedure consisted of geographical correction, land masking, ice-water discrimination, and the calculation of ice concentration. In order to avoid excess ice in the detection results caused by clouds, all the samples for validation were in clear weather condition. The average value of MODIS retrieval ice concentration in 625 pixels was taken as the validation data to assess AMSR-E retrieval result in each grid.

3 ARTIST SEA ICE ALGORITHM

The ASI algorithm (Spreen, et al., 2008) used the value of the polarization difference to derive ice concentration, and used low frequency data as weather filters to remove spurious ice c oncentration in open water areas and marginal ice zone.

First of all, the polarization difference P of the brightness temperatures of 89 GHz channel is calculated as below.

$$P = T_{bv} - T_{bh} \quad (1)$$

with T_{bv} for vertical polarization brightness temperatures and T_{bh} for horizontal polarization brightness temperatures. Assuming the atmospheric influence to be a smooth function of the ice concentration C, then a third-order polynomial is selected to fit the sea ice concentration between 0% and 100% with polarization difference.

$$C = d_3P^3 + d_2P^2 + d_1P + d_0 \quad (2)$$

Assuming that the tie-points of pure water and pure ice, expressed as P_0 and P_1 respectively, are known, two equations for pure water and pure ice conditions are obtained by taking them into Eq. (2). Then, by taking them into the first derivative formula of Eq. (2), another two equations can be acquired. It has been known that the polarization difference of the sea ice surface

[1] [2011-09-01] http://nsidc.org/data/amsre/order_data.html

were significantly smaller than that of the open water, and P equals to P_0 and P_1 when C is approaching 0 or 1. So, the quaternary linear equations (Spreen, et al., 2008) are derived to solve the four coefficients in Eq. (2) as below.

$$\begin{bmatrix} P_0^3 & P_0^2 & P_0 & 1 \\ P_1^3 & P_1^2 & P_1 & 1 \\ 3P_0^2 & 2P_0 & 1 & 0 \\ 3P_1^2 & 2P_1 & 1 & 0 \end{bmatrix} \cdot \begin{bmatrix} d_3 \\ d_2 \\ d_1 \\ d_0 \end{bmatrix} = \begin{bmatrix} 0 \\ 1 \\ -1.14 \\ -0.14 \end{bmatrix} \quad (3)$$

Given P_0 and P_1, d_0, d_1, d_2, and d_3 can be solved, and ice concentration C can be obtained as

$$C = 1.640 \times 10^{-5} P^3 - 1.618 \times 10^{-3} P^2 + 1.916 \times 10^{-2} P + 0.9710 \quad (4)$$

Meanwhile, it is demonstrated that if $P > P_0$, then $C = 0$; if $P < P_1$, then $C = 1$, thus the values of tie-points for pure water and pure ice surface (P_0 and P_1) have the direct impact on the retrieve results. Spreen, et al. (2008) determined the tie-points as $P_0 = 47$ K, $P_1 = 11.7$ K by comparing the ASI algorithm ice concentrations with ABA algorithm (comiso, et al., 2003) results and regulated the tie-points to make the minimal discrepancies. Although they showed that the P_0 and P_1 values vary seasonally, in the current version of AMSR-E ASI products published by University of Bremen, considering the temporal continuity, P_0 and P_1 are still defined to be constants as the values mentioned above.

Brightness temperature of AMSR-E 89 GHz is significantly affected by atmospheric conditions. The atmospheric water vapor, cloud liquid water, precipitation, wind-induced sea-particle and even rough surface can often lead to the surplus sea ice over open water or in adjacent of the edge of sea ice. Therefore, it is necessary to remove these potential sources of error in calculation. Currently, the weather filters used in ASI algorithm actually just rectified the mistakes of recognizing water surface as sea ice, but did not change the sea ice concentration values. There are three weather filters used in ASI algorithm (Spreen, et al., 2008):

The first weather filter uses the vertical polarization Gradient Ratio (GR) of the 36.5 GHz and 18.7 GHz channels. This ratio mainly considers the effects of cloud ice and cloud liquid water.

$$GR(37/19) = [T_b(37V) - T_b(19V)] / [T_b(37V) + T_b(19V)] \geqslant 0.045 \Rightarrow C = 0 \quad (5)$$

Second, to additionally exclude high water vapor cases above open water, the vertical polarization GR of 23.8 GHz and 18.7 GHz are used.

$$GR(23/19) = [T_b(23V) - T_b(19V)] / [T_b(23V) + T_b(19V)] \geqslant 0.04 \Rightarrow C = 0 \quad (6)$$

Finally, all ASI ice concentrations with corresponding ABA ice concentrations equal zero are set to zero.

Actually, the present weather filters only deal with the misjudgment of ice points, rather than adjusting the retrieval results. The points in retrieval field conforming to any term of the three filters would be set to be water. Technically, the threshold values of the weather filters should be spatially and temporally different. However our experimentsproved that by setting appropriate constant thresholds determined by statistical analysis, the above filters can work effectively under most conditions.

4 RETRIEVAL ALGORITHM EXPERIMENTS

From the AMSR-E ice concentration algorithm above we can see that the interpolation method, values of tie-points (P_0 and P_1) and the weather filters have direct impacts on the retrieval results. Therefore, in this study we performed a series of experiments including the interpolation algorithm, tie-points, and the weather filter based on the ASI algorithm, in order to lay the foundation of further improvement of the algorithm.

4.1 Interpolation algorithm test

AMSR-E L2A data, which consists of swath data of 29 channels per day, needs to be interpolated to generate grid data. In order to ensure the agreement with the previous products, we adopt the polar stereographic projection grid, with the coordinate origin point set at the North Pole and the standard latitude offset as 70°N. The grid resolution is 6.25 km. The latitude and longitude corresponding to each grid point are provided at the NSIDC website.

Seven tests on the interpolation algorithm were implemented, including the interpolation algorithm, map projection method, the effective swath width and the adjustment of the order of interpolation and projection, respectively. By comparing different combinations of the elements involved in the interpolation algorithm, we determined the algorithm which gave the minimal differentiation between the sea ice concentration result and that of University of Bremen. In the selected algorithm, the sea ice concentration retrieval steps were conducted with grid data in the same polar stereographic projection coordinates, which are acquired by the interpolation of swath data. When interpolating, the nearest point value assignment method was used, and if the nearest point was not unique, the latest measured value will be applied. According to the analysis by Spreen, et al. (2008), the difference between doing the inversion before or after interpolation was approximately 1%. The main reason we choose the former order is that gridded brightness temperature data can be generated at the same time. In addition, this scheme is more computationally efficient than the latter approach.

4.2 Tie-Points Test

According to the statistical analysis of AMSR-E data during 2003 to 2006 by Spreen, et al. (2008), the values of tie-points have obvious seasonal variations, and the amplitude of variation in Arctic is more than that in Antarctic. However, in their study, P_0 and P_1 were chosen by comparing the results from ASI and that from ABA (Comiso, et al., 2003). And this method is according the way what Kaleschke, et al. (2001) did on SSM/I data, that is, for different tie points value, calculating the spatial average of sea ice concentration error (MSE) between results of ASI algorithm and SSM/I NASA-Team Algorithm (Markus & Cavalieri, 2000). and chosing the tie points which coresponse to the multi-dimensional minimization on the MSE function. This method had the following problems: (1) it does not take into account of geographical factors; (2) it depends on the accuracy of NT deriving algorithm, causing interaction of the errors in two algorithms; (3) it is associated with the performances of weather filters; (4) it cannot reflect the true physical concept.

Therefore, it is necessary to perform statistical analysis of tie-points based on microwave remote data with physical feature.

The tie-points values of pure ice surface were sampled in multi-year ice area north of the Canadian Archipelago (84.0°N—85.0°N, 60.0°W—61.0°W), and that of pure water surfaces are sampled in area south of the Greenland ice edge (78.9°N—79.9°N, 7.0°E—8.0°E). For each day of 2009, the t ie-points values corresponding to the maximum probability in the probability distribution histograms of each area are selected as the tie-points values of that day, i. e. , P_0 and P_1, as shown in Fig. 1.

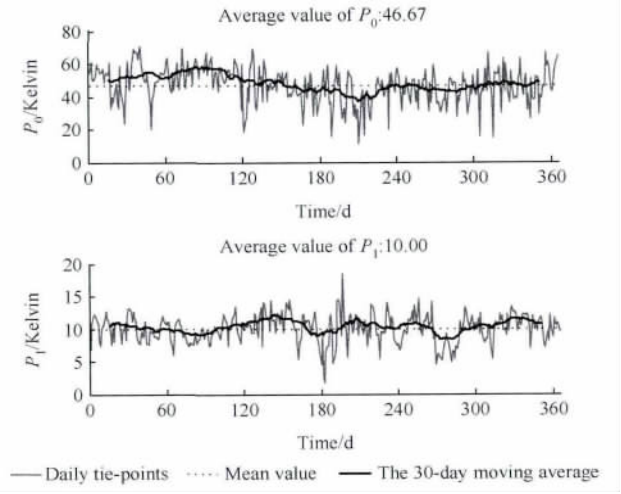

Fig. 1 Variations of P_0 (pure water tie-point, upper panel) and P_1 (pure ice tie-point, bottom panel) in sample region of Arctic in 2009

The average pure water tie-point (P_0) is 46.67 K in Arctic for the analysis in 2009, which is very close to that of Spreen's (2008) (47 K), and its standard deviation is 10.95 K. The average pure ice tie-point (P_1) is 10.00 K, which is lower by 1.7 K, and its standard deviation is 2.16 K. The annual amplitude of variation of P_0 is nearly five times that of P_1. This is due to: (1) the magnitude of the pure water pure ice tie-point values; (2) the sample area chosen for statistic the mean tie-points. The distance between the fixed sample area chosen for statistics of P_0 and the location of sea ice edge line is different seasonally. To this point, it is reasonable that this study selected the sample position in south of Greenland sea ice edge, where seasonal changes of the location of edge line are much smaller than that of other areas, such as the Bering Sea. Another reason may be due to the weather effect. The large anomalies of P_0 appeared in every season. The 30-day moving average time series of P_0 shows that higher values appear in March and April while lower values in July and August. The large anomalies of P_1 usually appear in July, August and September, among which the causes of positive values can be explained as the ice concentrations approaching 100% occurring in the pure ice region in summer, i. e. the impure sea ice in the selected area for tie-point statistics. The causes of the large negative anomalies will be further studied.

The tie-points acquired from statistics of the brightness temperature data are more reliable and physically reasonable than that derived from the comparison results of sea ice concentration inversion results using ASI and NASA TEAM algorithm, respectively. If we take the statistical tie-points into Eq. (3), the equation of ASI sea ice concentration will be changed to Eq. (7), which is different in the coefficients compared with Eq. (4).

$$C = 1.1983 \times 10^{-5} P^3 - 1.2 \times 10^{-3} P^2 + 5.6 \times 10^{-3} P + 1.0479 \quad (7)$$

The difference of sea ice concentrations calculated with Eq. (7) and Eq. (4) vary with changes of the brightness temperature p olarization difference P. The difference reaches its maximum (approximately 5%) when P is about 20 K. In order to further reveal the sensitivity of inversion results to the tie-points values, Fig. 2 shows the sea ice concentration inversion values corresponding to different P and tie-points difference ΔP_0 and ΔP_1, represented by the deviation values from the original system (P_0 = 47 K; P_1 = 11.7 K). Fig. 2 shows the significant sensitivity of the deriving results to the ΔP_0 and ΔP_1, especially when the d eviation is larger than 2 K. On one hand, when P_0 is small, the inversion result is sensitive to P ranging from 30 K to 42 K. The maximum underestimation of P is 17% when ΔP_0 equals −6 K. While P_0 is large, the significant differences appear with P r anging from 40 K to 48 K, and the maximum overestimation of 14% when P_0 equals 6 K. On the other hand, when P_1 is small, the inversion result is sensitive to P of 14—25 K, with the minimum underestimation of 18% appearing when ΔP_1 equals −6 K. When P_1 is large, the inversion value is sensitive to P of 20—2 8 K, with the maximum overestimation of 15% appearing when ΔP_1 equals 6 K. The conditions when P is smaller than 10 or ΔP_1 is larger than 3 (corresponding to the lower right corner) are not taken into our consideration, because under such conditions the ice concentration will be set to 100% in this inversion algorithm. Thus, acquiring a set of accurate tie-point values helps i mprove the inversion results.

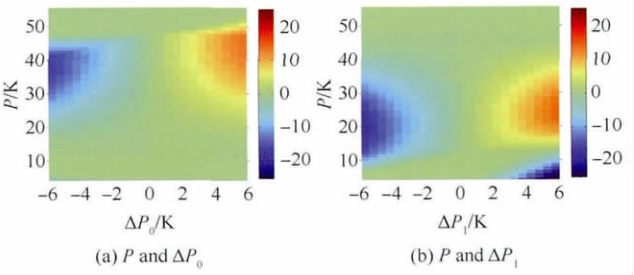

Fig. 2 Distribution of the difference(%) of the retrieved sea ice concentration from the original values (P_0 = 47 K, P_1 = 11.7 K) for different P and ΔP_0 or ΔP_1

4.3 Weather filter test

We implement tests of the first two weather filters described by Spreen, et al. (2008). The results show that, in summer both weather filters perform well, and most of the erroneous judgements caused by cloud and vapor can be removed. However, in winter the effect of GR (37/19) is better than that of GR (23/19). Fig. 3 gives the test in four different situations on October 28th, 2009. In the low-latitude areas, some spurious sea ice still exist after applying the two weather filters. To avoid the larger amount of calculation with the third weather filter, the overestimation of sea ice in areas outside the climatological sea ice region is set to be 0%; in other words, open water. Experiments showed this processing can get same effects of applying total three weather filters.

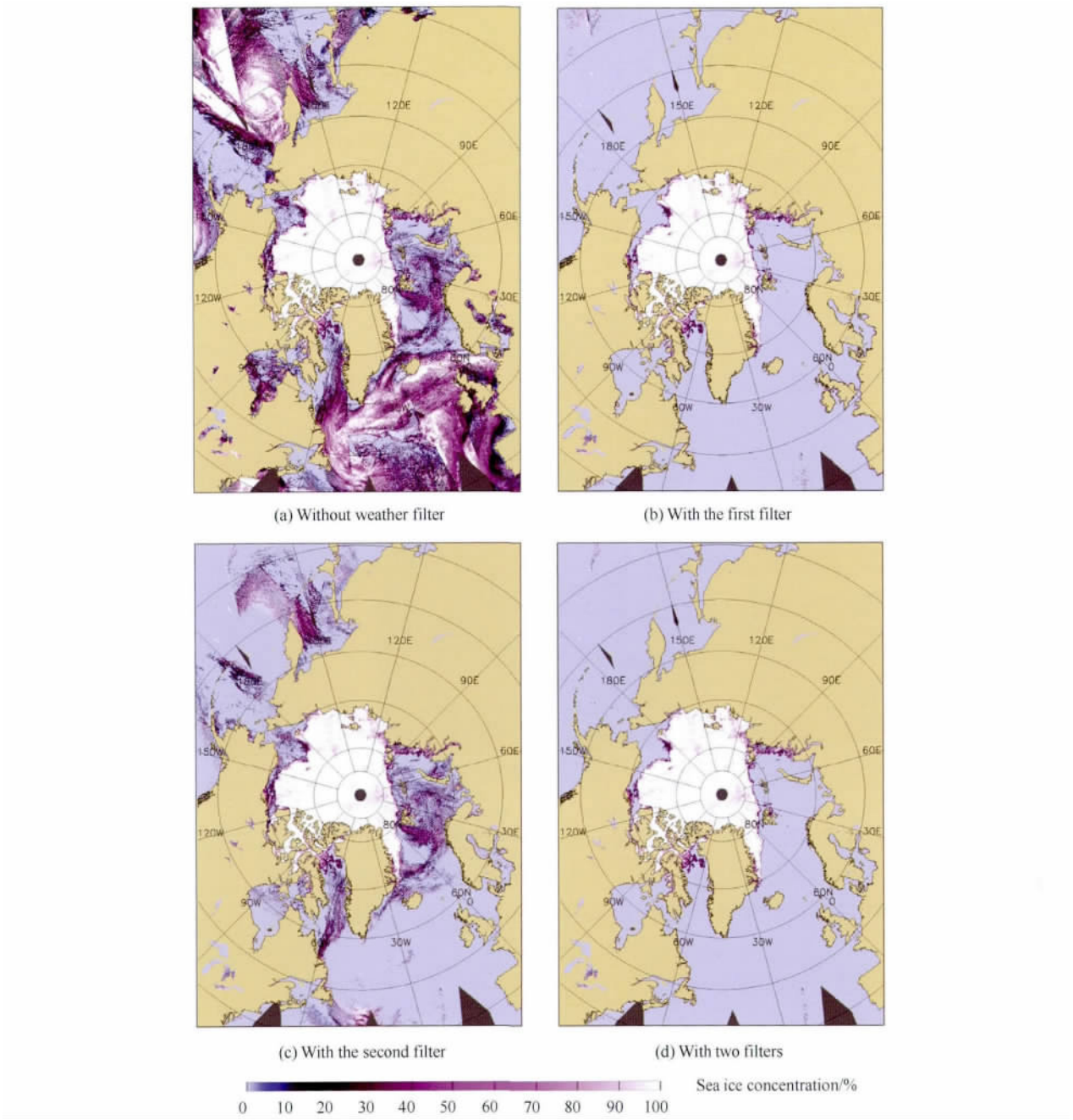

Fig. 3 Weather Filter Test on October 28th, 2009

5 COMPARISON AND VALIDATION

5.1 Comparison the retrieval product with the product of University of Bremen

Using Eq. (7), a 6.25 km resolution ice concentration remote sensing product is generated based on AMSR-E 89 GHz microwave data of year 2009. Compared with similar products of the University of Bremen, our results are generally smaller. The spatial average error is −0.26% and the average absolute error is 1.11% (Fig. 4). If the common water points which discriminated in two results were removed, the spatial average error is −3.5% to 1.5%, with the annual average of −1.15% and larger errors were observed in July to September. The average absolute error is also larger in summer and less in winter, and the annual average value is 4.66%. Fig. 5 shows the comparison of sea ice concentration distribution and their differences (our results against the Bremen's) in the period when mean absolute error is large (August 18th, 2009) and small (November 20th, 2009). The figure demonstrates that the sea ice distribution derived in this study is approximately similar to the products of the University of Bremen, and the differences mainly occur in areas adjacent to the sea ice edge. In summer, thin ice occupies larger area, thus the difference of two results is larger than that in other seasons.

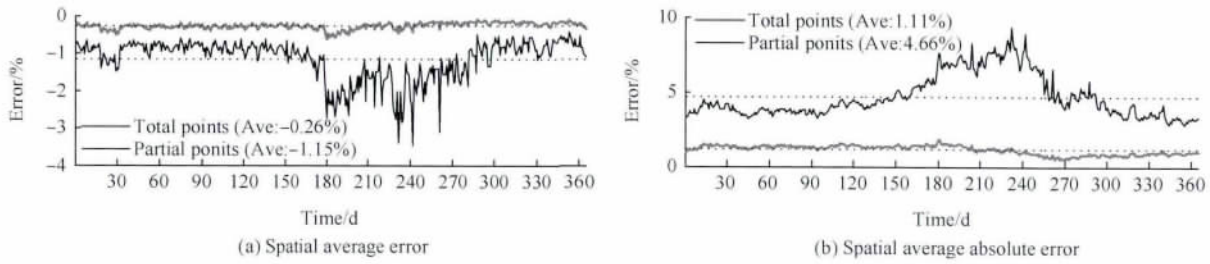

(a) Spatial average error (b) Spatial average absolute error

Fig.4 Error statistics between the retrieval results of this study and the University of Bremen's products in 2009

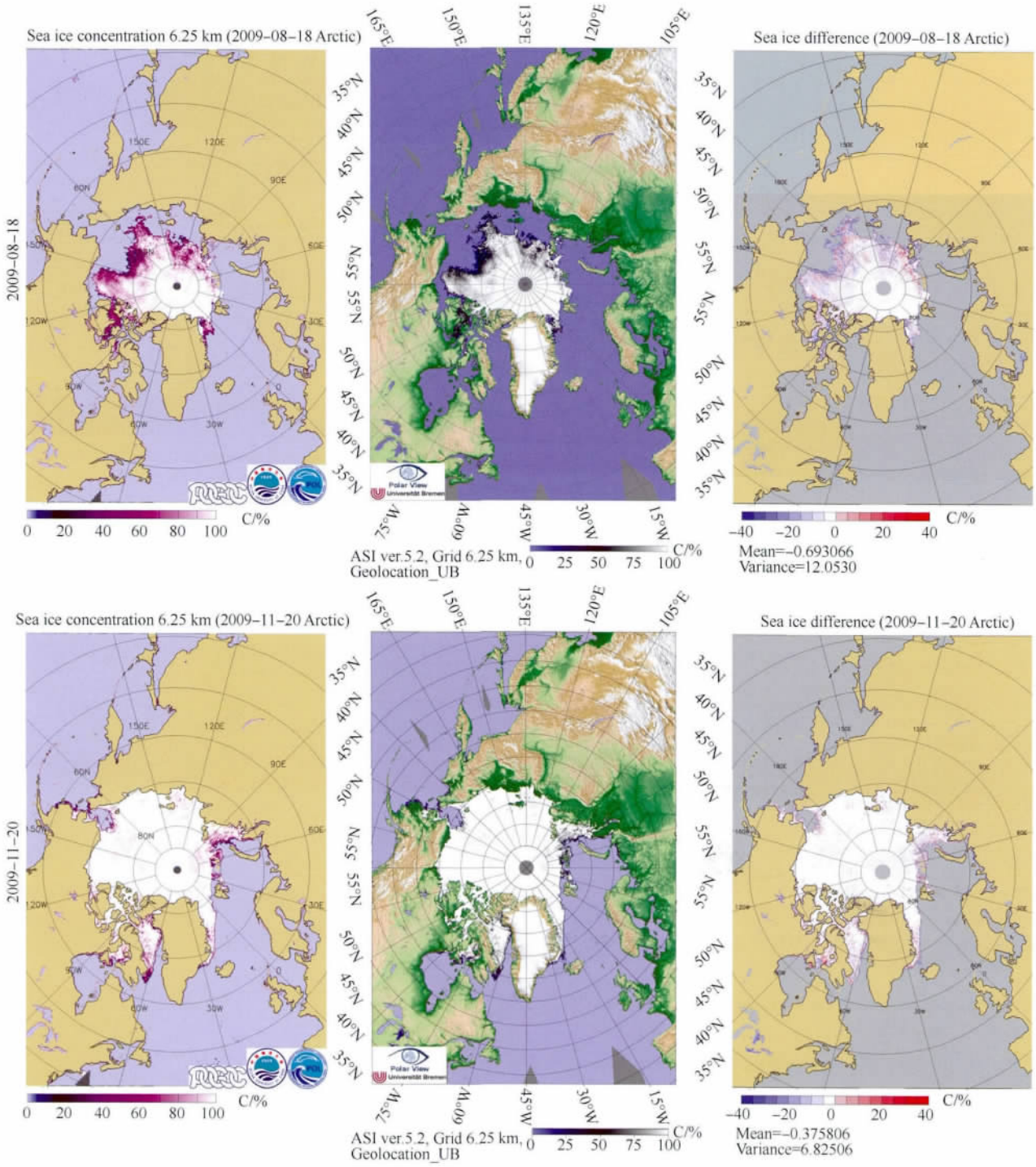

(a) Results of this study (b) Bremen products (c) Difference of this study and Bremen products

Fig.5 Arctic sea ice concentration distributions and difference of this study and products of the University of Bremen

5.2 Comparison with MODIS sea ice concentration

It is not an enough criterion to evaluate the retrieval results only by comparison with similar products. In this section, the visible light band of MODIS data is used to conduct further verification. First, in order to omit the error from the process of cloud detection and exclusion, we chose 12 MODIS samples u nder clear sky conditions. The time and locations of the selected samples of MODIS images are the same as Ye (2011) (Fig. 6). These samples are quite typical and representative, because they are mostly located in the marginal ice zone, where the seasonal variation of sea ice is apparent. In Ye, et al. (2011)'s study, a threshold algorithm is used for ice-water discrimination, then project each pixels onto the AMSR-E grid and the ice concentration is calculated by statistic ice points' proportion in each AMSR-E grid. The advantage of this algorithm is computationally efficient, but not accurate enough. Threshold algorithm is also used for ice-water discrimination in this paper, while the sea ice concentration value is retrieved from MODIS band 2 data using the traditional ice concentration retrieval fomula (Steffen, et al., 1991). Then the MODIS sea ice concentration in each pixel are interpolated and averaged onto the AMSR-E grid. The sea ice concentrations derived with this method are closer to the reality than those acquired by calculating ice proportion only base on ice-water discrimination result (Ye, et al., 2011).

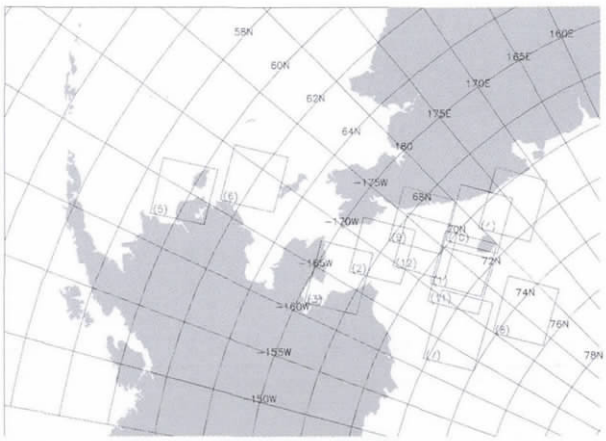

Fig. 6 Locations of the MODIS sample images chosen for validation (Ye, et al., 2011)
(1)—(3): 23:55 (UT), May 1st, 2009 (4): 23:30 (UT), May 21st, 2009 (5)—(6): 23:35 (UT), May 21st, 2009 (7)—(8): 00:15 (UT), May 23rd, 2009 (9)—(11): 23:20 (UT), May 23rd, 2009 (12): 23:45 (UT), June 4th, 2009

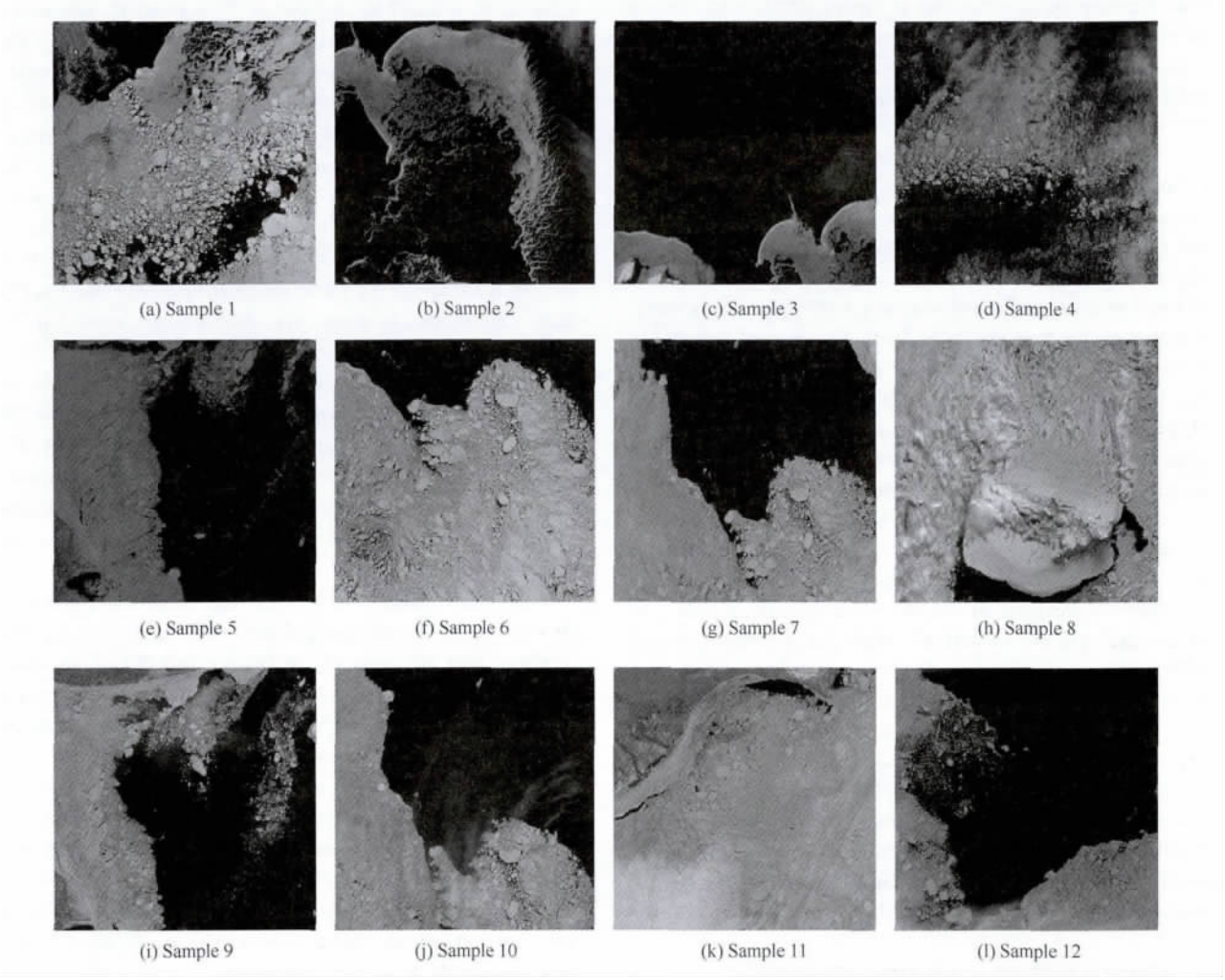

Fig. 7 MODIS band 2 gray scale images of 12 samples

Table 1 Statistical error of AMSR-E sea ice concentration and the MODIS results (ASI-MODIS) /%

Sample index	Bremen AE ($P_0=47, P_1=11.7$)	Ouc1 AE ($P_0=47, P_1=11.7$)	Ouc2 AE ($P_0=46.67, P_1=10.0$)	Bremen AAE ($P_0=47, P_1=11.7$)	Ouc1 AAE ($P_0=47, P_1=11.7$)	Ouc2 AAE ($P_0=46.67, P_1=10.0$)
1	15.88	1.98	4.65	23.11	16.31	19.29
2	5.85	1.86	0.94	13.47	10.23	11.07
3	4.75	1.99	1.72	6.53	4.13	4.61
4	10.41	1.47	0.39	14.04	10.59	11.85
5	7.28	5.88	4.21	10.10	9.99	9.87
6	11.98	7.73	7.26	12.50	10.48	9.90
7	5.59	2.23	2.66	12.19	14.12	12.10
8	15.12	12.57	10.10	16.51	15.48	15.12
9	6.59	3.70	1.58	10.93	9.89	10.57
10	7.36	3.37	4.06	9.29	6.60	7.44
11	8.76	6.52	4.44	10.37	9.84	9.14
12	7.71	1.79	4.11	10.10	7.27	9.16
Mean	8.94	4.26	3.84	12.43	10.41	10.83

Note: AE: Average Error; AAE: Average Absolute Error; Ouc: results of this study

Fig. 7 shows the MODIS band 2 gray scale images, in which white stands for ice surface and black for open water. The error statistics of the 12 samples are listed in Table 1. The first three columns in Table 1 correspond to the spatial averaged errors (AE) of three results of ASI sea ice concentration respectively, including Bremen products (Bremen), the results derived by using the same tie-points as that in Spreen (2008) (Ouc 1), and the results with the tie-points defined statistically in this paper (Ouc 2), compared with the MODIS ice concentration data. Similarly, the last three columns show the spatial Averaged Absolute Errors (AAE).

The validation results based on the 12 samples show that, compared with MODIS sea ice concentrations, the spatial averaged errors of Bremen, Ouc1 and Ouc2 are 8.94%, 4.26% and 3.84%, respectively; and the spatial averaged absolute errors of each results of ASI results are 12.43%, 10.41% and 10.83%. In terms of the spatial averaged errors, AMSR-E sea ice concentration is greater than that of MODIS. The error of sample 8 is maximal, with errors larger than 10% for all the three results. As shown in Fig. 6 and Fig. 7, this sample is located in northern part of the study area with thick and high concentration ice, so that some small and separated open water area may be neglected because of the coarser AMSR-E grid in the northern area, and the retrieved sea ice concentration is overall larger. In terms of the spatial averaged absolute errors, samples 1, 2, 4, 7, and 8 have larger errors than others. Among these samples, 1, 2, and 4 are under the condition of low sea ice concentrations with a lot of separated ice and unclear ice edges. Among these samples, thick fragmentary ice and melting ice are simultaneously present in sample 1. Sample No. 7 is also located in northern area with thick ice and high concentration, thus the cause of the higher error is similar to that of sample No. 8. In addition, the melting of sea ice surface in the microwave band has similar characteristics of open water. In particular, the small penetration depth of 89 GHz and ice melting is also influential for the results of AMSR-E data, such as samples 2 and 4. This is also one of the reasons for the differences of MODIS and AMSR-E results.

6 CONCLUSION AND DISCUSSION

Based on AMSR-E 89 GHz microwave data, a series of algorithm experiments, amendment and validations for ASI algorithm are implemented. The main results are listed as below.

(1) The tie-points of pure water (P_0) and pure ice (P_1) are statistically acquired by choosing the pure ice or water areas with the surface properties known, offering more reasonable values in physics for the retrieval algorithm. In 2009 the annual averaged value of P_0 is 46.67 K, and that of P_1 is 10.00 K. The annual variation amplitude of P_0 is nearly five times that of P_1. The sensitive experiments of tie-points show that, when the tie-point discrepancy is larger than 2 K, the difference of retrieved sea ice concentration is apparent. When P_0 or P_1 are small, their influences on the retrieved ice concentration are most obvious when P ranges from 30—42 K or 14—25 K. On the other hand, when P_0 or P_1 are large, the P values at which their influences on retrieved ice concentration are most obvious are ranges from 40—48 K or 20—28 K. The amended retrieval equation (Eq. (7)) from statistic the tie-points are favorable to improving the Spreen's (2008) retrieval performance.

(2) The weather filter experiments indicate that, the first two filters in Spreen's (2008) paper perform well in summer, but GR(37/19) is significantly superior to GR (23/19) in winter. The previous third weather filter can be replaced by setting the erroneously judged ice points outside the seasonally varied climatological sea ice edge line to be open water. And this will also save the computation time.

(3) Twelve samples of MODIS visible light band under the Arctic clear sky are selected and derived to validate the retrieval results of both the University of Bremen and that of our study. The comparisons indicate that, AMSR-E results are generally larger than the MODIS result. The relatively large spatial averaged errors and spatial average absolute errors usually occur in areas with the following characteristics: thick ice zone with a lot of small and separated water area; low ice concentration zone with separated ice; areas with unclear ice edge line; areas with fragmentary thick ice and thin melting ice simultaneously. From the statistical analysis for the MODIS samples in the marginal ice zone, we conclude that the accuracy of Ouc results are not lower than those of the University of Bremen (Table 1).

Through this study, sea ice concentration products were achieved from the AMSR-E brightness temperature swath data.

This work lays the foundation for releasing the quasi-real-time Chinese satellite monitoring products of polar sea ice concentrations. In this paper, we mainly focus on the Arctic region. In terms of the Antarctic region, the parameters of retrieval algorithm in this work cannot be directly used. The algorithm and its parameters may likely need to be amended in order to a chieve the Antarctic sea ice concentration deriving capability.

Validation of the microwave data derived results has always been a difficult problem. Most previous study used aerial p hotography or SAR inage analysis for verification. The use of aerial photography for verification, is limited by the aircraft altitude and the interval of shooting time, thus spatial consecutiveness can not be satisfied. This limitation causes the disagreement of spatial representativeness between aerial photographs and inversion results. SAR data need to be ordered in a dvance. In this paper, the MODIS inversion results was used to validate AMSR-E retrieval ice concentration. This enriched the ways of passive microwave inversion results validation. Of course, there are errors produced from the visible light radiation data as well as its retrieval algorithm of sea ice concentration. So, further research is needed on using integrated multiple sources verification data. In addition, the sea ice retrieval results are still not satisfying in the marginal ice zone, because of the low spatial resolution of microwave data. Therefore, the study on merging the data of microwave and visible light sensors in the marginal ice zone might be one of the crucial methods of improving the accuracy of sea ice concentration inversion.

Acknowledgements: Thanks to Mrs. Heidi Maass for her help on the English editing of this paper.

REFERENCES

Andersen S, Tonboe R, Kaleschke L, Heygster G and Pedersen L T. 2007. Intercomparison of passive microwave sea ice concentration retrievals over the high-concentration Arctic sea ice. Journal of Geophysical Research: Oceans, 112(C8) 1 - 18 [DOI: 10.1029/2006JC003543]

Cavalieri D, Gloersen P and Campbell W. 1984. Determination of sea ice parameters with the Nimbus 7 SMMR. Journal of Geophysical Research: Atmospheres, 89(D4): 5355 - 5369 [DOI: 10.1029/JD089iD04p05355]

Comiso J C. 1986. Characteristics of arctic winter sea ice from satellite multispectral microwave observations. Journal of Geophyspheric R esearch: Oceans, 91 (C1): 975 - 994 [DOI: 10.1029/JC091iC01p00975]

Comiso J C. 1995. SSM/I ice concentrations using the bootstrap algorithm. Greenbelt, MD, NASA Goddard Space Flight Center Ref. Publication, No. 1380, 40

Comiso J C, Cavalieri D J and Markus T. 2003. Sea Ice Concentration, ice temperature, and snow depth using AMSR-E data. IEEE Transactions on Geoscience and Remote Sensing, 41(2): 243 - 252 [DOI: 10.1109/TGRS.2002.808317]

Kaleschke L, Lüpkes C, Vihma T, Haarpaintner J, Bochert A, Hartmann J and Heygster G. 2001. SSM/I sea ice remote sensing for mesoscale ocean-atmosphere interaction analysis: Ice and icebergs. Canadian Journal of Remote Sensing, 27(5): 526 - 537

Kern S. 2001. A new algorithm to retrieve the sea ice concentration using weather-corrected 85 GHz SSM/I measurements. Bremen: Dept. Physics Elect. Eng. Univ. Bremen: 1 - 5

Kern S and Heygster G. 2001. Sea-ice concentration retrieval in the antarctic based on the SSM/I 85. 5 GHz polarization. Annals of Glaciology, 33(1): 109 - 114

Kern S, Kaleschke L and Clausi D A. 2003. A comparison of two 85 GHz SSM/I ice concentration algorithms with AVHRR and ERS - 2 SAR imagery. IEEE Transactions on Geoscience and Remote Sensing, 41(10): 2294 - 2306 [DOI: 10.1109/TGRS.2003.817181]

Markus T and Cavalieri D J. 2000. An enhancement of the NASA Team sea ice algorithm. IEEE Transactions on Geoscience and Remote Sensing, 38(3): 1387 - 1398 [DOI: 10.1109/36.843033]

Spreen G, Kaleschke L and Heygster G. 2008. Sea ice remote sensing u sing AMSR-E 89-GHz channels. Journal of Geophysical Research: Oceans, 113(C2) [DOI: 10.1029/2005JC003384]

Steffen K and Schwieger A. 1991. NASA Team algorithm for sea ice concentration retrieval from defense meteorological satellite program special sensor Microwave/Imager: Comparison with landsat satellite imagery. Journal of Geophysical Research, 96(C12): 21971 - 21988

Svendsen E, Matzler C and Grenfell T. 1987. A model for retrieving total sea ice concentration from a spaceborne dual-polarized passive microwave instrument operating near 90 GHz. International Journal of Remote Sensing, 8 (10): 1479 - 1487 [DOI: 10.1080/01431168708954790]

Ye X X, Su J, Wang Y, Hao G H and Hou J Q. 2011. Assessment of AMSR-E sea ice concentration in ice margin zone using MODIS data. International Conference on Remote Sensing Environment and Transportation Engineering (proseeding). Nanjing: IEEE, 5: 3869 - 3873 [DOI: 10.1109/RSETE.2011.5965163]

极区海冰密集度 AMSR－E 数据反演算法的试验与验证

苏洁[1]，郝光华[1]，叶鑫欣[1,2]，王维波[1]

1. 中国海洋大学 教育部物理海洋重点实验室,山东 青岛 266100;
2. 北京大学 物理学院大气与海洋科学系,北京 100871

摘 要: 海冰密集度是极区海冰监测的重要参数,目前分辨率最高的微波海冰密集度产品为德国 Bremen 大学发布的针对 AMSR-E 89 GHz 频段数据利用 ASI 算法反演的网格数据。为实现中国极区遥感产品从无到有的战略步骤,本文针对 AMSR-E 89GHz 频段微波数据的 ASI 算法,进行了插值算法、系点值和天气滤波器一系列试验。针对北极海区,着重对影响反演结果的主要参数——纯冰和纯水的亮温极化差异阈值,即系点值(P_1 和 P_0)进行了 2009 年全年的统计分析。研究表明,2009 年北极纯冰和纯水的代表区域 P_1 和 P_0 年平均值分别为 10.0 K 和 46.67 K;2 K 以上的系点值差异引起的海冰密集度差别较为显著;同样的系点值差异在不同极化差异 P 取值范围对海冰密集度的影响也不同。通过统计确定的系点值推算并修正了海冰密集度反演公式,对 2009 年全年北极海冰密集度进行了反演,并与 Bremen 大学产品进行了比较。继而对白令海和楚科奇海 12 个晴空下 MODIS 可见光样本数据进行反演,以验证 AMSR-E 冰密集度反演结果,并对误差原因进行了分析。本研究反演结果与 MODIS 样本比对的误差略小于 Bremen 大学的反演产品,空间平均误差为 3.84%,空间平均绝对误差 10.83%。

关键词: AMSR-E,海冰密集度,反演算法,验证,极区

中图分类号: TP701/P731.15 **文献标志码**: A

引用格式: 苏洁,郝光华,叶鑫欣,王维波. 2013. 极区海冰密集度 AMSR-E 数据反演算法的试验与验证. 遥感学报,17(3): 495－513

Su J, Hao G H, Ye X X and Wang W B. 2013. The experiment and validation of sea ice concentration AMSR-E retrieval algorithm in polar region. Journal of Remote Sensing, 17(3): 495－513

1 引 言

极区是全球气候的指示器,随着全球变暖日益加剧,海冰作为极区重要的气候因子,其监测和研究受到越来越多的关注。海冰密集度是描述海冰特征的重要参数之一,也是大气和海洋环流模式的输入参数,它描述海冰的空间密集程度,指一定范围内海冰所占的面积百分比。目前国际上可用于大面积海冰密集度监测和反演的卫星传感器主要有主动和被动微波辐射计、可见光和红外辐射计及成像光谱仪等。微波数据具有不受昼夜限制、受云雾影响较小及较好的时空连续性等特点,已成为极区海冰监测的重要手段。

卫星数据的分辨率和反演算法对准确地提供海冰密集度至关重要。目前分辨率最高的微波数据产品是德国 Bremen 大学利用微波扫描辐射计 AMSR-E(Advanced Microwave Scanning Radiometer-Earth Observing System)的 89 GHz 高频数据反演的 6.25 km 分辨率的海冰密集度格点化产品(Spreen 等,2008)。目前针对 AMSR-E 数据的海冰密集度反演算法多是根据针对分辨率较低的特殊传感器微波图像仪 SSM/I(Special Sensor Microwave Imager)数据的算法按相应波段应用到 AMSR-E 数据的。Andersen 等人(2007)曾总结了针对 SSM/I 数据的 7 种海冰密集度的反演算法。目前应用较多的海冰密集度反演算法中,NASA-Team 算法(Cavalieri 等,

收稿日期: 2012-02-14; 修订日期: 2012-09-24; 优先数字出版日期: 2012-10-01

基金项目: 国家高技术研究发展计划(863 计划)(编号: 2008AA121701)

第一作者简介: 苏洁(1966—),女,博士,副教授,现主要从事冰－海耦合和海冰遥感方面的研究。E-mail: sujie@ouc.edu.cn

1984) 和 Bootstrap 算法(Comiso, 1986, 1995) 是基于 19 GHz 和 37 GHz 频段数据的低分辨率反演算法; NASA-Team2 算法(Markus 和 Cavalieri, 2000) 、SEA LION 算法(Kern, 2001; Kern 和 Heygster, 2001) 和 ARTSIST Sea Ice (ASI) (Kaleschke 等, 2001) 等算法中都包括了 SSM/I 85 GHz 频段的数据,可生成 1 2.5 km分辨率的密集度数据。其中, ASI 算法产生于 1998 年的北极辐射与湍流相互作用研究(Arctic Radiation and Turbulence Interaction Study) ARTSIST 项目,该算法是对 Svendsen 等人(1987) 提出的近 90 GHz 频段数据的海冰密集度反演算法的改进(Kaleschke 等, 2001) 。ASI 算法与其他近 85 GHz 频段的算法相比,具有不需要额外的数据源的优点,而且与利用其他通道的海冰密集度算法有相似的结果(Kern 等, 2003) 。

AMSR-E 89 GHz 频段的空间分辨率达到 4 km × 6 km,近似为 SSM/I 在 85 GHz 频段的分辨率(13 km × 15 km) 的 3 倍。因此,AMSR-E 数据发布后,人们迅速将 SSM/I 相应频段的海冰密集度的反演算法应用到 AMSR-E 数据。基于 AMSR-E 数据的 ASI(Spreen 等, 2008) 、NASA-Team2 和 AMSR Bootstrap Algorithm (ABA) (Comiso 等, 2003) 的反演结果与 2003 年 3 月—4 月和 2004 年 7 月—8 月(航线代号分别为 ARK-XIX/1 和 ARK-XX/2) "北极星"号考察船船舶观测数据的相关系数分别为 0 .80、0.79 和 0. 81; 2002 年—2006 年期间 ASI 的结果(6. 25 km) 与 NASA-Team2 结果(12.5 km) 偏差为 - 2 ± 8. 8% ,与 ABA(12.5 km) 结果偏差为 1.7 ± 10.8% ,反映了 ASI 算法的有效性(Spreen 等, 2008) 。同时, ASI 算法由于采用了 89 GHz 的数据,可提供 6 .25 km的密集度产品,比 NASA-TEAM2 和 ABA 算法对应的产品分辨率(12.5 km) 高一倍。

将原始轨道数据插值到产品网格,是反演流程的基本步骤,插值方式会对逐日海冰密集度场的反演结果有一定影响。虽然 ASI 反演算法已发表,但插值算法却没有具体说明; 同时,ASI 算法中确定系点值(即纯冰和纯水的亮温极化差异的阈值) 的前提条件是令反演出的海冰密集度结果与 ABA 算法(Comiso 等, 2003) 的结果最接近(Spreen 等, 2008) 。这种做法无疑会使 ASI 算法的反演结果受到 ABA 算法反演结果精度的影响; 另外,与低频段数据相比,89 GHz 频段数据容易受到大气中的水汽(如云滴、雨滴等) 干扰,特别是在薄冰区,当云中液态水含量高或有气旋经过时,反演结果误差较大; 同时对海冰表面积雪颗粒密度的大小也十分敏感,基于 8 9 GHz数据的 ASI 算法中需要包括天气滤波器,以滤掉冰边缘区以外误判为海冰的水汽等成分(Spreen 等, 2008) 。基于以上原因,本文对 ASI 算法进行进一步试验并对反演结果进行准确性验证,并在此基础上改进了算法。国家高技术研究发展计划重点项目"极区海冰与海洋过程遥感监测技术",将应用、发展研制海冰密集度等 16 项极区海冰和海洋遥感参数的反演算法,实现极区遥感产品从无到有,并最终实现极区遥感产品的准业务化发布。在此背景下,本文针对 AMSR-E 89 GHz 频段微波数据的 ASI 算法进行了插值算法、系点值和天气滤波器试验,进而讨论系点值对反演结果的影响,通过统计修正了系点值,并利用 MODIS 可见光数据对反演结果进行了验证。

2 数据来源

源数据主要是美国国家冰雪数据中心 NSIDC (National Snow and Ice Data Center) [1] 发布的 AMSR-E L2A 轨道亮温数据。AMSR-E 是搭载在 AQUA 卫星平台、于 2002 年 5 月发射的被动微波辐射计,能够测量地球表面在 89. 0 GHz, 3 6.5 GHz, 2 3.8 GHz,18.7 GHz,10.7 GHz 和 6.9 GHz 频段水平和垂直极化通道的被动微波亮温。下载了国际上同类产品,即 Bremen 大学发布的 AMSR-E 海冰密集度 6.25 km 产品(Spreen 等, 2008) ,用于算法的初步比对。

主要验证数据为 MODIS 可见光遥感数据。MODIS 提供 0.4—14.5 μm 的 36 个离散波段的图像,视场宽度为 2330 km,能够清晰、实时地给出地表和海表面环境状况。本文选取 AQUA-MODIS 传感器 250 m 分辨率 L1B 第 2 通道数据,采用系点法(Steffen 和 Achwieger, 1991) 进行海冰密集度反演。其中数据处理步骤包括: 地理订正、陆地掩膜应用、冰水识别和冰密集度反演计算,为了避免云检测判断的误差,选择晴空条件下的个例进行验证。对应每个 AMSR-E 网格(包括 625 个 MODIS 格点) ,对 MODIS 反演结果进行网格平均,作为评价微波数据海冰密集度反演结果的验证数据。

[1] [2011 - 09 - 01] http: //nsidc. org/data/amsre/order_data,html

3 ASI 算法简介

ASI 算法(Spreen 等,2008)利用 89 GHz 水平和垂直极化差异对海冰密集度进行反演,并采用低频亮温作为天气过滤器,去除由于气旋等天气过程产生的水汽引起的在冰外缘带密集度低值区和无冰区域的误判。

首先计算 89 GHz 的亮温极化差异:

$$P = T_{bv} - T_{bh} \tag{1}$$

式中,T_{bv}表示垂直极化的亮温,T_{bh}表示水平极化的亮温。假设大气对海冰密集度的影响是光滑函数,可用一个关于 P 的三次多项式拟合从 0% 到 100% 的海冰密集度:

$$C = d_3P^3 + d_2P^2 + d_1P + d_0 \tag{2}$$

假设纯水和纯冰的系点值是已知的,分别表示为 P_0 和 P_1,代入式(2)可得到纯水和纯冰的两个方程,再对式(2)求导,也分别代入纯水和纯冰的条件。已知冰面的极化差异显著小于开阔水面的极化差异,且海冰密集度 C 趋近 0 和 1 时极化差异 P 分别为 P_0 和 P_1,得出用于求解式(2)系数的四元一次线性方程组,见式(3),推导过程详见参考文献(Spreen 等,2008)。

$$\begin{bmatrix} P_0^3 & P_0^2 & P_0 & 1 \\ P_1^3 & P_1^2 & P_1 & 1 \\ 3P_0^2 & 2P_0 & 1 & 0 \\ 3P_1^2 & 2P_1 & 1 & 0 \end{bmatrix} \cdot \begin{bmatrix} d_3 \\ d_2 \\ d_1 \\ d_0 \end{bmatrix} = \begin{bmatrix} 0 \\ 1 \\ -1.14 \\ -0.14 \end{bmatrix} \tag{3}$$

根据式(3)可求解 d_0,d_1,d_2,d_3,代入式(2)便可计算海冰密集度 C:

$$C = 1.640 \times 10^{-5}P^3 - 1.618 \times 10^{-3}P^2 + 1.916 \times 10^{-2}P + 0.9710 \tag{4}$$

同时规定,若 $P > P_0$,则 $C = 0$;若 $P < P_1$,则 $C = 1$。可见纯水和纯冰的系点值 P_0 和 P_1 对反演结果有直接影响。Spreen 等人(2008)通过对比 ASI 算法与 ABA 算法(Comiso 等,2003)的海冰密集度结果,将极化差异特征点值固定为 $P_0 = 47$ K,$P_1 = 11.7$ K。虽然他们指出 P_0 和 P_1 的值具有季节性变化,但考虑到海冰反演结果的时间连续性,在目前 Bremen 大学发布的 AMSR-E 产品算法中,P_0 和 P_1 仍采用以上常数。

AMSR-E 89 GHz 频段的亮温受大气现象影响显著,大气中水蒸气、云中液态水、降水粒子及风引起的海面粗糙不平会导致在开阔海面和海冰的边缘的无冰海面计算出海冰。因此需要将这部分误判去除。Spreen 等人(2008)使用的 3 种天气滤波器为:

(1)利用 36.5 GHz 和 18.7 GHz 垂直极化亮温的光谱梯度率 GR(Gradient Ratio)滤去云中冰晶和液态水的影响:

$$GR(37/19) = [T_b(37V) - T_b(19V)] / [T_b(37V) + T_b(19V)] \geqslant 0.045 \Rightarrow C = 0 \tag{5}$$

(2)利用 23.8 GHz 和 18.7 GHz 垂直极化亮温的光谱梯度率 GR(23/19)滤去开阔水面上水蒸气的影响:

$$GR(23/19) = [T_b(23V) - T_b(19V)] / [T_b(23V) + T_b(19V)] \geqslant 0.04 \Rightarrow C = 0 \tag{6}$$

(3)将 ABA 算法冰密集度为 0 处的冰密集度反演结果直接赋值为 0。

目前 ASI 算法中使用天气滤波器只是去除了那些被误判为海冰的水点,并没有改变冰点的海冰密集度值。满足其中任意一种滤波器的点都可判为水点。天气滤波器的阈值也应该是随时空变化的,但经本文试验证明,通过统计确定的以上常数阈值可以满足大部分情况。

4 反演算法试验

从以上 AMSR-E 算法分析可知,插值算法、P_0 和 P_1 值及天气滤波器对反演结果有直接影响。因此,本研究针对 AMSR-E 89 GHz 频段微波数据的 ASI 算法,进行了插值算法试验、系点值试验和天气滤波器试验,为进一步改进该算法打下基础。

4.1 插值算法试验

AMSR-E 数据每天有 29 轨数据,需要利用插值算法从轨道数据生成格点数据。为了和国际上已有产品一致,密集度反演结果数据的地理网格也取为极地立体投影网格,坐标原点位于北极点,标准纬线为 70°N,网格分辨率 6.25 km,每个格点所对应的经纬度数据由 NSIDC 网站提供。

本文进行了 7 组试验,包括插值算法、映射投影方向、轨道有效宽度和插值、投影顺序调整,通过比对插值组合方案,最终确定了与 Bremen 冰密集度产品的差异最小的方案。采用最近点赋值;轨道相互叠加时取最上层轨道数据,即生成时间最晚的轨道数据;先将轨道亮温数据插值到相同的极地立体投影坐标下,再进行反演。试验表明,先对轨道亮温数

据做反演运算,再将结果插值到相同的极地立体投影坐标网格下与先插值再反演的密集度结果差别约为 1%(Spreen 等,2008)。我们选择先插值投影再反演的流程的主要原因,一是可以同时生成亮温格点数据,二是要保证计算效率。

4.2 系点值试验

根据 Spreen 等人(2008)对 2003 年—2006 年 AMSR-E 数据的统计分析研究,系点值具有明显的季节变化,而且北极比南极变化幅度大。但是在他们的研究中,P_0 和 P_1 值是通过比较 ASI 算法和 ABA 算法(Comiso 等,2003)反演结果选取的。这种做法是根据基于 SSM/I 数据的 ASI 算法系点值选取方法进行的,即将 ASI 算法(Kaleschke 等,2001)和 NASA TEAM2 算法(Markus 和 Cavalieri,2000)计算海冰密集度的平均空间误差(MSE)函数做多维最小化,使 MSE 达到最小。该方法存在以下问题:(1)没有考虑地理因素;(2)与 NASA-Team2 算法或 ABA 算法反演精度有关,算法间误差相互影响;(3)与滤波器有关;(4)不能最好地反映真实物理概念。

因此,有必要对纯冰和纯水的系点值进行更具有物理意义的统计分析。我们对 2009 年北极逐日的 P_0 和 P_1 值进行统计。其中纯冰点样本取在加拿大群岛以北多年冰区(84.0°N—85.0°N,60.0°W—61.0°W),纯水点样本取在格林兰海冰外缘线以南海区(78.9°N—79.9°N,7.0°E—8.0°E);分别计算两个区域的极化差异、进行概率分布统计,选取逐日最大概率发生的值,作为当天的极化差异值,即 P_0 和 P_1(图 1)。

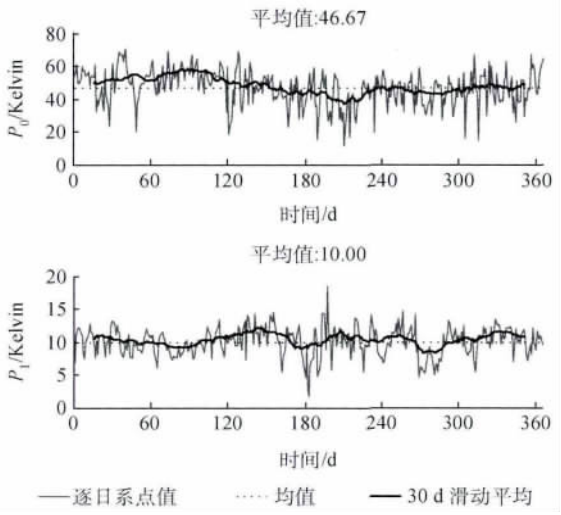

图 1 2009 年北极 P_0 值(纯水系点)和 P_1 值(纯冰系点)

2009 年北极区域纯水系点值(P_0)平均为 46.67 K,与 Spreen 等人(2008)给出的值非常接近(47 K),标准差为 10.95 K;纯冰系点值(P_1)平均为 10.00 K,标准差为 2.16 K。比 Spreen 等人给出的 11.7 K小 1.7 K。统计的 P_0 值比 P_1 值在一年内的变化大近 5 倍,这一方面与冰点和水点的亮温值大小有关,另一方面也与进行系点值统计时选取的样本区域有一定关系。在不同的季节所选纯水区域的位置离冰外缘线的距离有差别,从这点讲,我们将纯水点夏季取在格林兰海冰外缘线以南海区是合理的,因为这里的冰外缘线位置季节性变化比白令海等其他海区要小得多。P_0 值在每个季节都有较大的距平出现,从 30 d 滑动平均时间序列看,总体在 3、4 月份值较高,7、8 月份值较低;P_1 值较大的距平多出现在 7 月—9 月,其中偏大的值可以解释为夏季纯冰点样本区域海冰密集度可能出现小于 100%,也就是非纯冰的情况;偏小值的成因还需进一步研究。

根据亮温数据统计的系点值比依靠反演的海冰密集度与 NASA TEAM 算法结果最接近条件下选定的参数更具物理意义,将统计系点值代入式(3),所得到的海冰密集度计算公式与式(4)相比系数发生改变,如式(7)所示。

$$C = 1.1983 \times 10^{-5} P^3 - 1.2 \times 10^{-3} P^2 + 5.6 \times 10^{-3} P + 1.0479 \quad (7)$$

式(7)与式(4)计算的海冰密集度的差别随表面极化亮温 P 变化,当 P 为 20 K 左右时差别最大,海冰密集度相差近 5%。

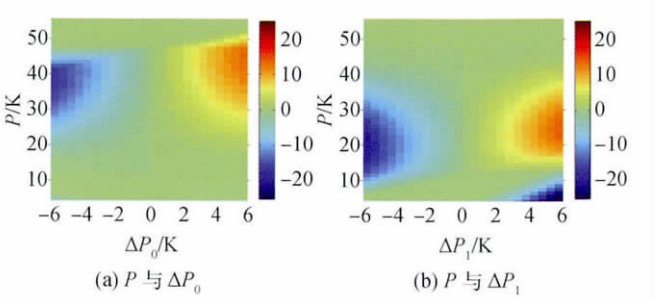

图 2 不同极化差 P 及 ΔP_0 和 ΔP_1 对应的相对于标准系点值的海冰密集度差值/%

为了进一步揭示反演结果对系点值的敏感程度,图 2 给出了对应不同的 P 值、系点值差异 ΔP_0 和 ΔP_1 的海冰密集度反演结果相对原系点值(P_0 = 47 K;P_1 = 11.7 K)反演结果的偏差。由图可见,当 ΔP_0 和 ΔP_1 大于 2 K 时,对密集度结果影响较大。P_0 偏小时,P_0 对密集度反演结果的影响最大出现在

P 值为 30—42 K 的范围,当 ΔP_0 为 -6 K 时,密集度较取标准值偏小达 17%; P_0 偏大时,P_0 对密集度反演结果的影响最大,对应的 P 值为 40—48 K,当 ΔP_0 为 6 K 时,密集度较取标准值偏大达 14%; P_1 偏小时,P_1 对密集度反演结果的影响最大出现在 P 值为 14—25 K 的范围,当 ΔP_1 为 -6 K 时,密集度较取标准值偏小可达 18%; P_1 偏大时,P_1 对密集度反演结果的影响最大对应的 P 值为 20—28 K,当 ΔP_1 为 6 K 时,密集度较取标准值偏大达 15%。

小于 10 的 P 值和 ΔP_1 大于 3 的情况(对应图中右下角的数据)可以不必考虑,因为在试验中当 P_1 较大时,小于该值的 P 值会被定义为纯冰,而不等于式(7)计算的值。由此可见,选取准确的系点值将对反演结果的提高有利。

4.3 天气滤波器试验

根据 Spreen 等人(2008)的研究,分别对前两种滤波器进行试验(图 3),试验结果显示,夏季多数情

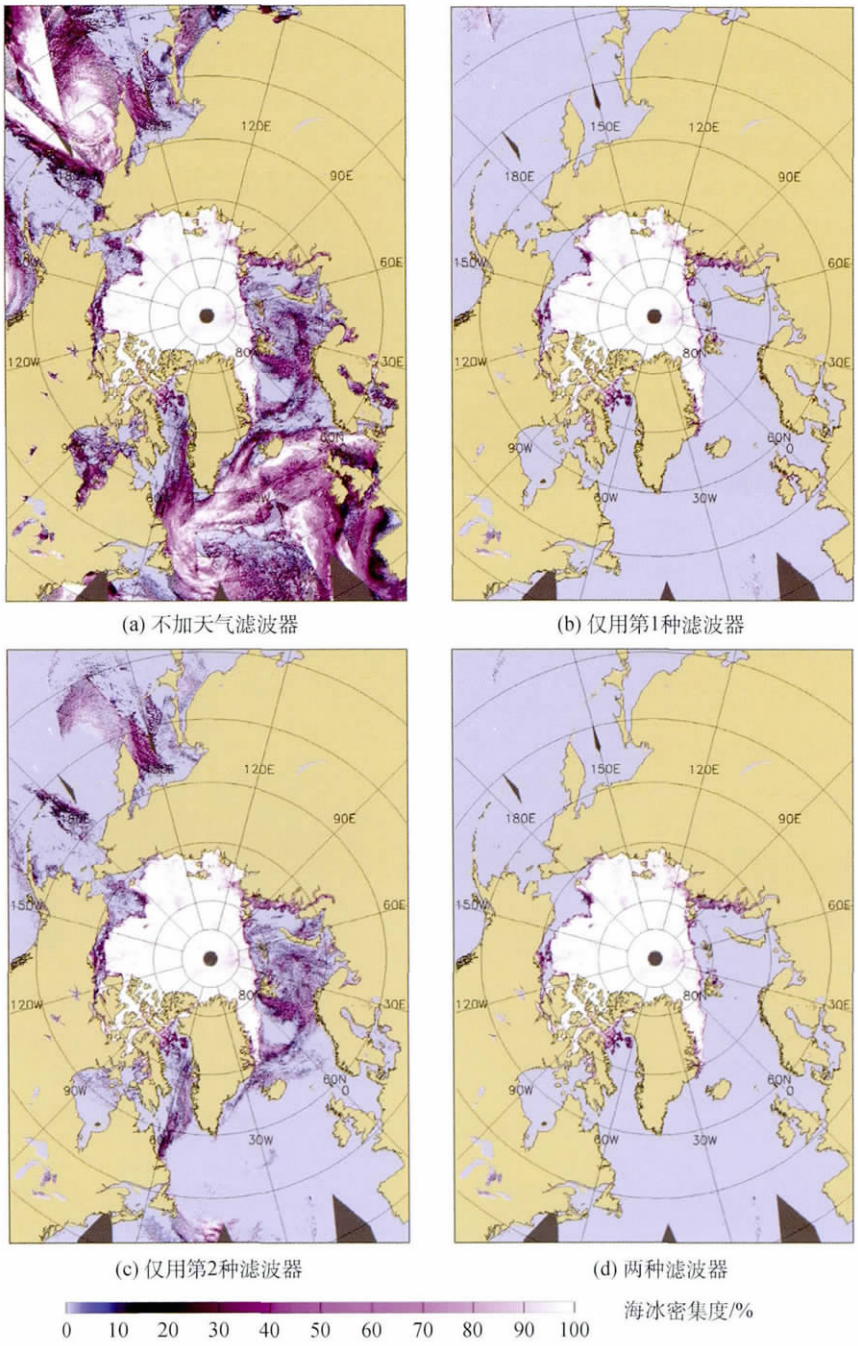

图 3 2009 -10 -28 天气滤波器试验

况下,两种天气滤波器的效果都较好,能够去除绝大多数的云和水汽; 但在冬季,第 1 种滤波器 GR(37/19) 的效果明显优于 GR(23/19) 。在使用两种滤波器后,低纬地区仍存在少量误判,第 3 种滤波器需要嵌入 ABA 算法,增加计算量,因此,本文只采用两种滤波器,对于远在气候态冰外缘线之外的区域,如果出现误判为海冰的情况,则判为开阔水域。试验表明这种简单的处理方法能够代替第 3 种天气滤波器,达到同样的效果。

5 反演结果的比对和验证

5.1 与 Bremen 大学产品的比较

在 IDL 语言和软件环境下,利用式(7) 计算海冰密集度,生成了 2009 年全年的基于 AMSR-E 89 GHz微波辐射数据的 6.25 km 海冰密集度遥感产品。与 Bremen 大学同类产品比较(图 4) 可以看出,本文结果较整体偏小。整个北极全场空间平均误差和空间平均绝对误差很小,分别只有 -0.26% 和 1.11% 。若将两个结果中同时判为的水点的部分去掉进行统计,空间平均误差基本为 -3.5%—1.5% ,全年平均误差为 -1.15% ,其中 7 月—9 月误差较大; 空间平均绝对误差也体现出夏季较大、冬季较小的特点,全年平均误差为 4.66% 。图 5 和图 6 分别给出了绝对误差较大时段(2009 -08 -18) 和误差较小时段(2009 -11 -20) 的反演结果及 Bremen 大学产品的差值场。由图可见,本研究反演的海冰密集度空间分布与 Bremen 同类产品近似程度很高,主要的差别还是发生在冰边缘区的低密集度分布海区,夏季海冰密集度较小的区域增大,两种产品的偏差也随之增大。

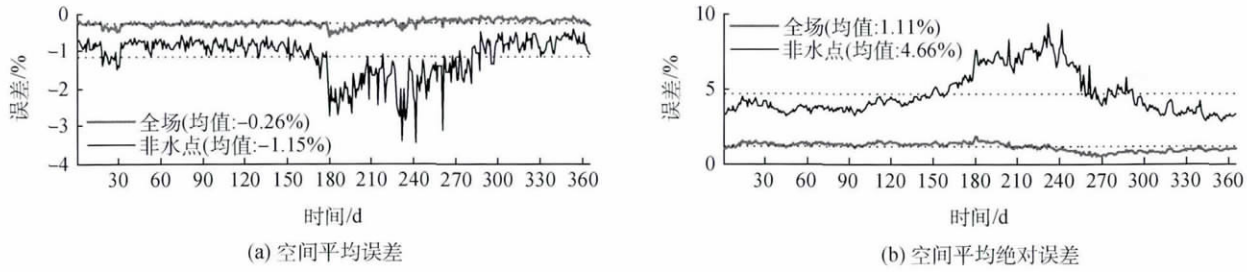

图 4 2009 年本研究反演结果与 Bremen 大学北极密集度产品的误差统计

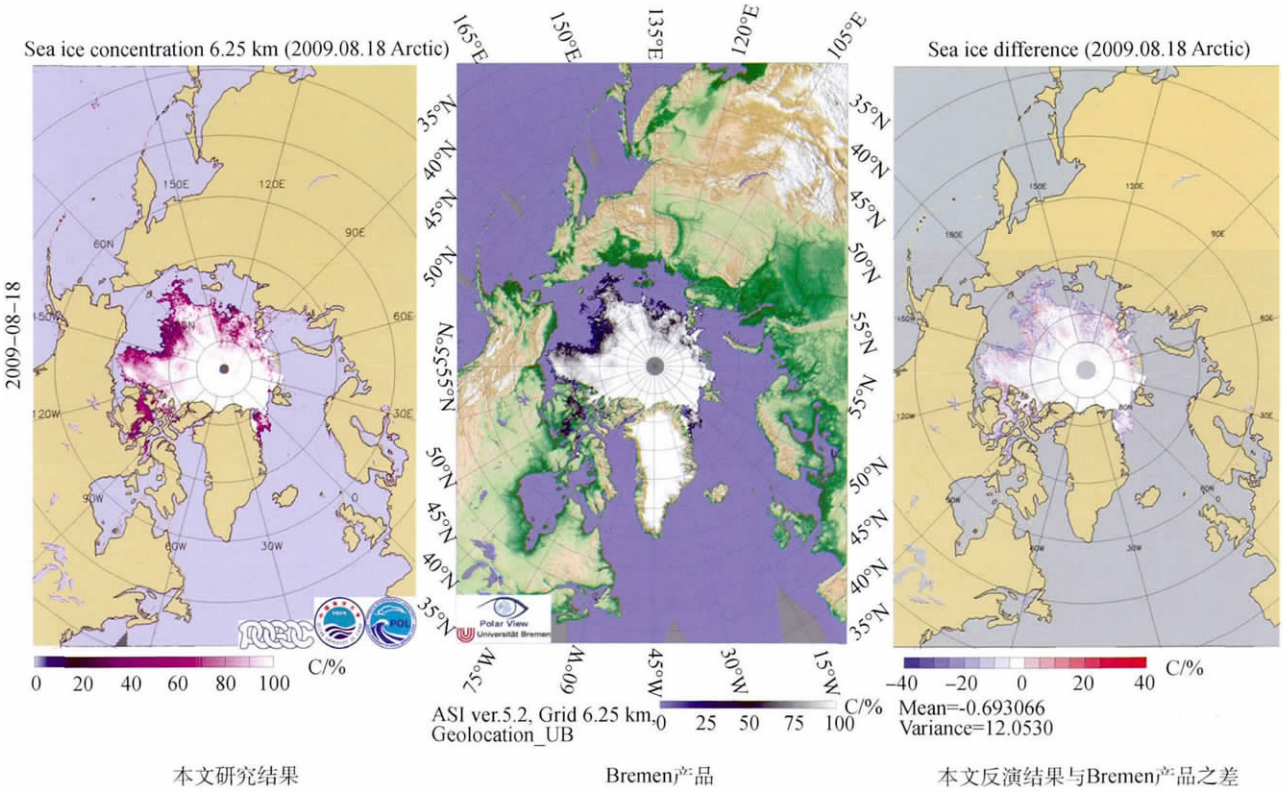

图 5 2009 年 8 月 18 日北极海冰密集度反演场和 Bremen 大学产品的比较

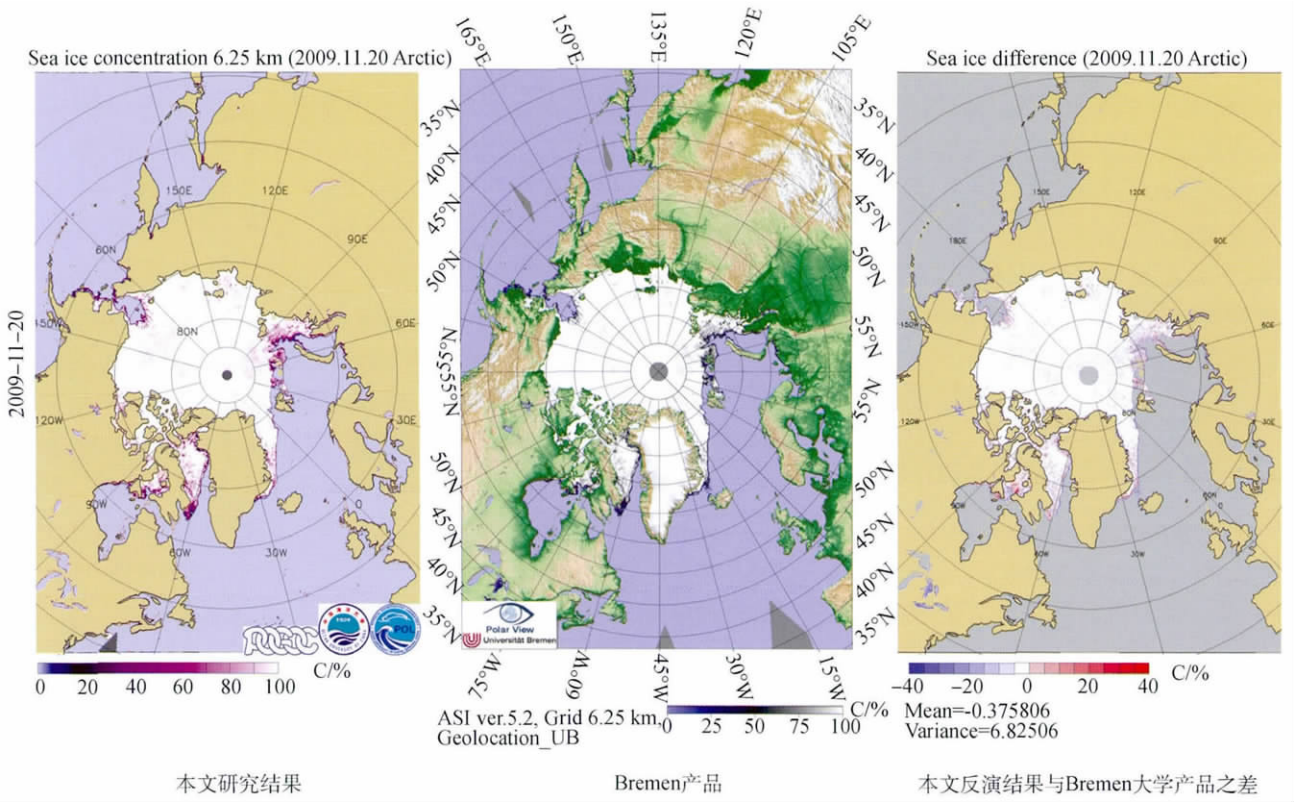

图 6 2009 年 11 月 20 日北极海冰密集度反演场与 Bremen 大学产品的比较

5.2 与 MODIS 反演海冰密集度的比对验证

由于与 Bremen 大学产品差别的大小只代表与国际同类产品的比较情况,并不能作为最终的误差检验标准,因此,接下来利用 MODIS 可见光通道数据对密集度反演结果进行进一步验证。首先从 MODIS 图像中挑选晴空下的个例,这样可以免除云剔除处理过程所带来的误差。我们所选取的 12 个例与 Ye 等人(2011)相同,时间和位置见图 7。这些样本区域基本分布在海冰边缘区,是季节性海冰变化的典型区域,具有很好的代表性。Ye 等人(2011)对 MODIS 可见光图像进行冰水识别后,将各像元点直接投影到 AMSR-E 网格,通过统计冰点和水点的个数,计算基于 MODIS 数据的海冰密集度。这种做法的优点是计算效率高,但不够准确。本文利用第 2 通道 250 m 分辨率数据进行冰水识别,继而利用传统的密集度反演公式(Steffen 等,1991)进行反演,继而将每个 MODIS 格点的密集度在 AMSR-E 网格下进行平均,以此来验证 AMSR-E ASI 算法得到的海冰密集度。这种反演方法得到的 MODIS 数据密集度值比 Ye 等人(2011)方法更接近实际。

图 8 给出了各样本区域 250 m 分辨率的 MODIS 第 2 通道的灰度图,其中白色为海冰,黑色为开阔水面。表 1 给出了这 12 个样本的误差统计结果。表中前 3 列分别为 Bremen 大学产品、采用与 Spreen 等人(2008)相同的系点值和采用本文统计系点值的本文反演结果(分别记为 Ouc1 和 Ouc2)与 MODIS 反演结果的空间平均误差;后 3 列为上述 3 种海冰密集度结果与 MODIS 反演结果的空间平均绝对误差。

图 7 MODIS 波段 2 灰度图子区域地理位置(Ye 等,2011)
(1)—(3):2009-05-01 23:55(UT);(4):2009-05-21 23:30(UT);(5)—(6):2009-05-21 23:35(UT);(7)—(8):2009-05-23 00:15(UT);(9)—(11):2009-05-23 23:20(UT);(12):2009-06-04 23:45(UT)

12 个样本的验证结果显示,AMSR-E 海冰密集

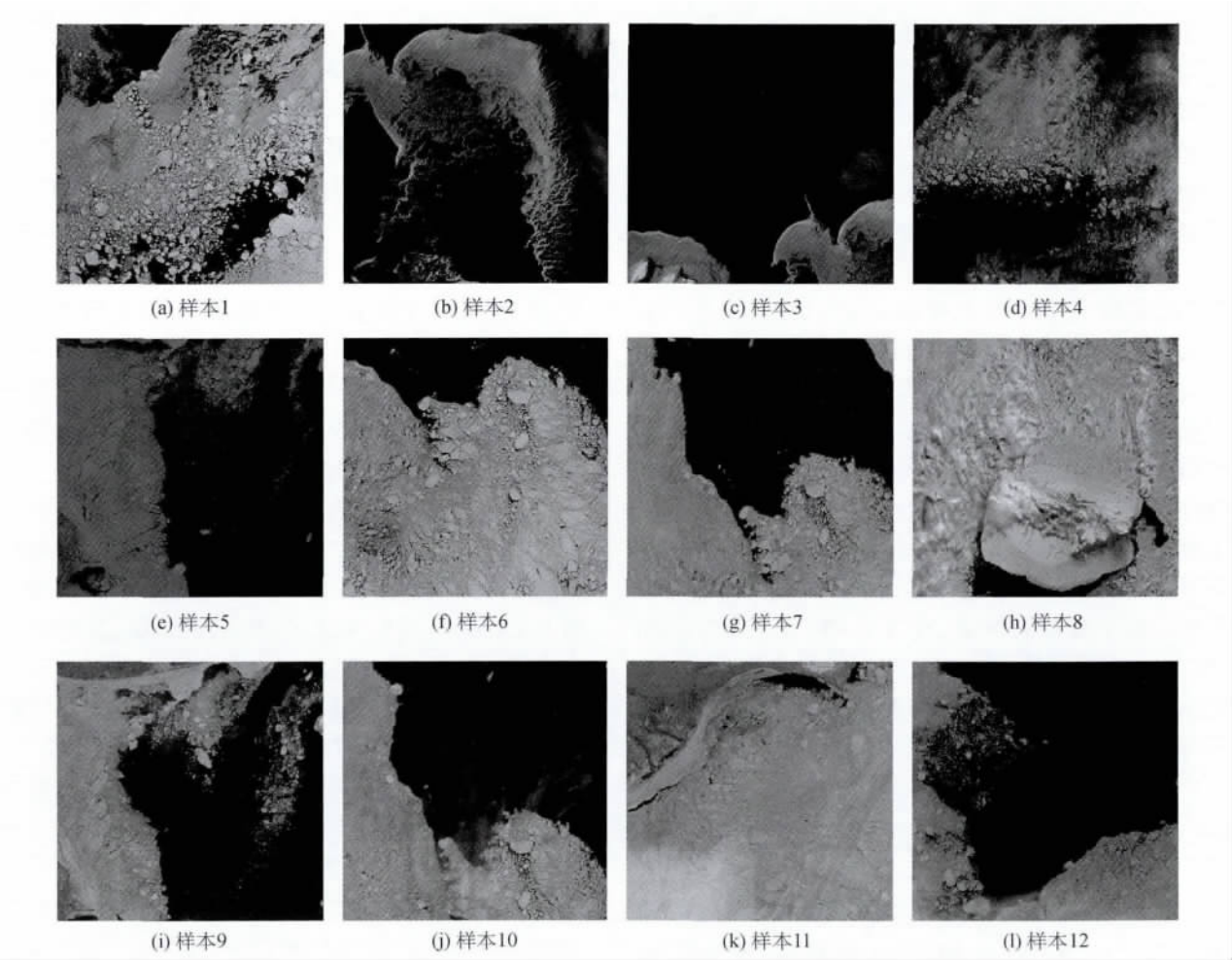

图 8　12 个样本区域的 MODIS 灰度图

表 1　AMSR-E ASI 与 MODIS 海冰密集度比对误差(ASI-MODIS)　/%

图像序号	Bremen 平均误差 ($P_0=47, P_1=11.7$)	Ouc1 平均误差 ($P_0=47, P_1=11.7$)	Ouc2 平均误差 ($P_0=46.67, P_1=10.0$)	Bremen 平均绝对误差 ($P_0=47, P_1=11.7$)	Ouc1 平均绝对误差 ($P_0=47, P_1=11.7$)	Ouc2 平均绝对误差 ($P_0=46.67, P_1=10.0$)
1	15.88	1.98	4.65	23.11	16.31	19.29
2	5.85	1.86	0.94	13.47	10.23	11.07
3	4.75	1.99	1.72	6.53	4.13	4.61
4	10.41	1.47	0.39	14.04	10.59	11.85
5	7.28	5.88	4.21	10.10	9.99	9.87
6	11.98	7.73	7.26	12.50	10.48	9.90
7	5.59	2.23	2.66	12.19	14.12	12.10
8	15.12	12.57	10.10	16.51	15.48	15.12
9	6.59	3.70	1.58	10.93	9.89	10.57
10	7.36	3.37	4.06	9.29	6.60	7.44
11	8.76	6.52	4.44	10.37	9.84	9.14
12	7.71	1.79	4.11	10.10	7.27	9.16
平均值	8.94	4.26	3.84	12.43	10.41	10.83

度反演结果与 MODIS 可见光图像统计结果的空间平均误差 Bremen、Ouc1 和 Ouc2 分别为 8.94 %、4.26% 和 3.84%,空间平均绝对误差分别为 12.43%、10.41% 和 10.83%。就空间平均误差而言,AMSR-E 反演的密集度均大于 MODIS 反演结果,其中样本 8 误差最大,3 种方法都超过了 10%。由图 7 和图 8 可见,样本 8 位置偏北,海冰密集,由于 AMSR-E 网格较粗,会忽略掉一些较小的、分散的水区,使得反演的海冰密集度整体偏大。从空间平均绝对误差看,样本 1、2、4、7 和 8 误差较大,其中 1、2 和 4 是密集度较小、碎冰较多、且冰水的分界线模糊的情况,而且在样本 1 中厚的碎冰和较薄的融冰同时存在;样本 7 海冰分布虽然远小于样本 8,但都属于海冰很密集的情况,造成误差的原因基本相同。另外,海冰表面的融化(如融池)也可能在微波波段产生类似于水面的特征,特别是 89 GHz 穿透深度小,海冰的融化对 AMSR-E 判识结果也有影响,如样本 2 和 4 的情况。这也是 MODIS 与 AMSR-E 结果差异的原因之一。

6 结 论

针对 AMSR-E 89 GHz 微波数据的 ASI 算法,进行了一系列算法试验、修正和验证,主要结论如下:

(1) 统计已知表面性质区域的纯水系点值和纯冰系点值,可以为反演算法提供更符合物理意义的系点值参数;2009 年北极代表区域纯水系点值(P_0)平均为 46.67 K,纯冰系点值(P_1)平均为 10.00 K,统计的 P_0 值比 P_1 值在一年内的变化大近 5 倍;系点值的敏感度试验表明,在系点值相差 2 K 以上时,对应的海冰密集度反演结果差别比较显著,P_0(P_1)偏小时,P_0(P_1)对密集度反演结果的影响最大出现在 P 值为 30—42 K(14—25 K)的范围,P_0(P_1)偏大时,P_0(P_1)对密集度反演结果的影响最大对应的 P 值为 40—48 K(20—28 K)的 P 值。选取准确的系点值对反演结果的提高有利,本文通过统计系点值,修正了 Spreen 等人(2008)的反演公式。

(2) 天气滤波器试验表明,GR(37/19)和 GR(23/19)两种天气滤波器在夏季效果都较好,但在冬季滤波器 GR(37/19)的效果明显优于 GR(23/19)。根据季节变化的气候态外缘线位置,加入判定远在冰区之外的区域为冰点的限制,可以代替原算法中复杂的嵌入 ABA 算法的第 3 种滤波器,达到同样的效果,并可节省计算量;

(3) 选取了北极区域 12 个晴空下 MODIS 可见光数据进行海冰密集度反演,得到在 AMSR-E 格点下的海冰密集度,利用该结果分别对 Bremen 大学和本研究反演的海冰密集度产品进行了比对验证,AMSR-E 结果总体密集度大于 MODIS 反演结果,平均误差和绝对平均误差较大的样本具有以下特点:带有小的、分散水区的密集冰区;含有较多碎冰的低密集度冰区;冰水的分界线模糊的区域;厚的碎冰和较薄的融冰同时存在的区域。从海冰边缘区样本的误差统计结果看,本研究反演结果的精度均不低于国际同类产品(表 1)。

通过本研究,实现了从轨道亮温数据生成极区海冰密集度反演产品,为实现中国极区海冰密集度卫星监测准实时产品发布打下基础。本文主要介绍了北极海冰的反演试验、修正和验证,我们对南极海冰也做了反演,目前正在对产品进行验证。对南极区域,不能直接套用北极的反演参数,需要做进一步统计,甚至是算法修正。

微波遥感数据反演结果的验证一直是个困难的问题,以往多采用航拍照片或 SAR 图像分析等进行验证。利用航拍数据和现场拍摄照片验证受到飞机飞行高度、拍摄时间间隔的影响,使拍摄的照片空间不连续,存在着比对验证“点对面”空间尺度不一致的问题。而 SAR 数据需要提前订购。本文采用 MODIS 反演结果作为 AMSR-E 反演海冰密集度的验证数据,丰富了微波数据的验证方法。但是,用于验证的可见光数据及其冰密集度反演方法本身也存在一定的误差。还需要进一步研究如何综合利用多种验证数据。另外,由于微波数据受到分辨率的限制,其反演结果在冰边缘区难以令人满意,因此,在海冰边缘区开展微波辐射计数据与较高分辨率的可见光/红外辐射计数据融合研究,或许是改进海冰密集度的反演准确率的重要途径之一。

参考文献(References)

Andersen S, Tonboe R, Kaleschke L, Heygster G and Pedersen L T. 2007. Intercomparison of passive microwave sea ice concentration retrievals over the high-concentration Arctic sea ice. Journal of Geophysical Research: Oceans, 112(C8) 1 - 18 [DOI: 10.1029/2006JC003543]

Cavalieri D, Gloersen P and Campbell W. 1984. Determination of sea ice parameters with the Nimbus 7 SMMR. Journal of Geophysical Re-

search: Atmospheres, 89(D4): 5355 - 5369 [DOI: 10.1029/JD089iD04p05355]

Comiso J C. 1986. Characteristics of arctic winter sea ice from satellite multispectral microwave observations. Journal of Geophyspheric Research: Oceans, 91 (C1): 975 - 994 [DOI: 10.1029/JC091iC01p00975]

Comiso J C. 1995. SSM/I ice concentrations using the bootstrap algorithm. Greenbelt, MD, NASA Goddard Space Flight Center Ref. Publication, No. 1380, 40

Comiso J C, Cavalieri D J and Markus T. 2003. Sea Ice Concentration, ice temperature, and snow depth using AMSR-E data. IEEE Transactions on Geoscience and Remote Sensing, 41(2): 243 - 252 [DOI: 10.1109/TGRS.2002.808317]

Kaleschke L, Lüpkes C, Vihma T, Haarpaintner J, Bochert A, Hartmann J and Heygster G. 2001. SSM/I sea ice remote sensing for mesoscale ocean-atmosphere interaction analysis: Ice and icebergs. Canadian Journal of Remote Sensing, 27(5): 526 - 537

Kern S. 2001. A new algorithm to retrieve the sea ice concentration using weather-corrected 85 GHz SSM/I measurements. Bremen: Dept. Physics Elect. Eng. Univ. Bremen: 1 - 5

Kern S and Heygster G. 2001. Sea-ice concentration retrieval in the antarctic based on the SSM/I 85. 5 GHz polarization. Annals of Glaciology, 33(1): 109 - 114

Kern S, Kaleschke L and Clausi D A. 2003. A comparison of two 85 GHz SSM/I ice concentration algorithms with AVHRR and ERS - 2 SAR imagery. IEEE Transactions on Geoscience and Remote Sensing, 41(10): 2294 - 2306 [DOI: 10.1109/TGRS.2003.817181]

Markus T and Cavalieri D J. 2000. An enhancement of the NASA Team sea ice algorithm. IEEE Transactions on Geoscience and Remote Sensing, 38(3): 1387 - 1398 [DOI: 10.1109/36.843033]

Spreen G, Kaleschke L and Heygster G. 2008. Sea ice remote sensing using AMSR-E 89-GHz channels. Journal of Geophysical Research: Oceans, 113(C2) [DOI: 10.1029/2005JC003384]

Steffen K and Schwieger A. 1991. NASA Team algorithm for sea ice concentration retrieval from defense meteoro1ogica1 satellite program special sensor Microwave/lmager: Comparison with landsat satellite imagery. Journal of Geophysical Research, 96 (Cl2): 2 1971 - 21988

Svendsen E, Matzler C and Grenfell T. 1987. A model for retrieving total sea ice concentration from a spaceborne dual-polarized passive microwave instrument operating near 90 GHz. International Journal of Remote Sensing, 8 (10): 1479 - 1487 [DOI: 10.1080/01431168708954790]

Ye X X, Su J, Wang Y, Hao G H and Hou J Q. 2011. Assessment of AMSR-E sea ice concentration in ice margin zone using MODIS data. International Conference on Remote Sensing Environment and Transportation Engineering (proseeding). Nanjing: IEEE, 5: 3869 - 3873 [DOI: 10.1109/RSETE.2011.5965163]